PHYSICAL REVIEW C **93**, 011304(R) (2016)

Microscopic modeling of mass and charge distributions in the spontaneous fission of ^{240}Pu

Jhilam Sadhukhan,[1,2] Witold Nazarewicz,[2,3] and Nicolas Schunck[4]
[1]*Physics Group, Variable Energy Cyclotron Centre, 1/AF Bidhan Nagar, Kolkata 700064, India*
[2]*Department of Physics and Astronomy and FRIB Laboratory, Michigan State University, East Lansing, Michigan 48824, USA*
[3]*Institute of Theoretical Physics, Faculty of Physics, University of Warsaw, 02-093 Warsaw, Poland*
[4]*Nuclear and Chemical Science Division, Lawrence Livermore National Laboratory, Livermore, California 94551, USA*
(Received 24 October 2015; published 20 January 2016)

We propose a methodology to calculate microscopically the mass and charge distributions of spontaneous fission yields. We combine the multidimensional minimization of collective action for fission with stochastic Langevin dynamics to track the relevant fission paths from the ground-state configuration up to scission. The nuclear potential energy and collective inertia governing the tunneling motion are obtained with nuclear density functional theory in the collective space of shape deformations and pairing. We obtain a quantitative agreement with experimental data and find that both the charge and mass distributions in the spontaneous fission of ^{240}Pu are sensitive both to the dissipation in collective motion and to adiabatic fission characteristics.

DOI: 10.1103/PhysRevC.93.011304

Introduction. Spontaneous fission (SF) is fundamental radioactive decay of very heavy atomic nuclei [1]. In basic science, it is a major driver determining the stability of the heaviest and superheavy elements [2–4]. Information on SF rates and fission fragment distributions are key ingredients of reaction network calculations aimed at simulating the formation of elements in the universe through nucleosynthesis processes [5–8]. In the context of the nuclear data program, SF data are crucial for calibration of nuclear material counting techniques relevant to international safeguards [9,10]. Since the discovery of SF in 1940, considerable experimental effort has been devoted to obtaining precise data on SF observables such as fission half-lives, fission yield properties (charge, mass, excitation energy, etc.), and γ and particle spectra. However, many nuclei relevant to nuclear astrophysics are very short lived and out of experimental reach. Moreover, measurements in actinide nuclei for nuclear technology applications can pose safety issues. Theory is, therefore, indispensable to fill in the gaps in nuclear data libraries.

Modeling SF represents a daunting theoretical challenge. Fission is an extreme manifestation of quantum tunneling in a many-body system of strongly interacting particles. Since fission is believed to be a fairly slow process driven by a few collective degrees of freedom, the most advanced theoretical efforts today are often based on the adiabatic approximation as implemented in nuclear density functional theory (DFT). This approach has proven successful in describing SF half-lives [11–14], but has rarely been considered for the distribution of charge, mass, and kinetic energy of the SF yields [15]. Even semiphenomenological models of fission dynamics have been mostly focused on neutron- and γ-induced fission and electron-capture delayed fission but not SF [16–22]. Today, empirical scission-point models are the only tools available to calculate SF fragment distributions [8,23].

Within the DFT picture, the evolution of the nuclear system in SF can be viewed as a dynamical two-step process. The first phase is tunneling through a multidimensional PES. The dynamics of this process, primarily adiabatic, is governed by the collective fission inertia. Beyond the outer turning point, the system propagates in a classically allowed region before reaching scission, where it finally breaks into two fragments. The motion in the second phase has a dissipative character. Consequently, the microscopic description of SF should involve potential, inertial, and dissipative aspects [24,25].

Although the tunneling phase could be described by instanton methods, which would account for some form of dissipation between collective and intrinsic degrees of freedom [26–28], numerous difficulties plague practical applications of the imaginary-time approach [29]. Consequently, most DFT-based calculations of tunneling probabilities are based on the semiclassical WKB approximation and depend sensitively on the interplay between the static nuclear potential energy and the collective inertia.

The characterization of fission yields poses additional challenges. At scission, dissipation plays a crucial role and would be best accounted for by time-dependent density functional theory (TDDFT). It is only very recently that realistic time-dependent Hartree-Fock calculations of the fission process have become available [30,31]. Albeit very promising, the current implementations of TDDFT treat several important aspects of nuclear structure (center of mass, nuclear superfluidity) rather crudely and cannot always properly describe collective correlations [32]. In addition, such calculations can only simulate single fission events: reconstructing the full mass distribution in TDDFT is beyond current computational capabilities, since it would involve large-scale Monte Carlo sampling of all possible fragmentations. Fortunately, such a sampling is easily doable within the classical Langevin dynamics [33].

The present work is an important milestone for our long-term project aiming at providing an accurate description of SF within nuclear DFT. Recently, we demonstrated that the predicted SF pathways essentially depend on the assumptions behind the treatment of collective inertia and collective action [34] (see also recent Ref. [35]). In Ref. [36], we also showed

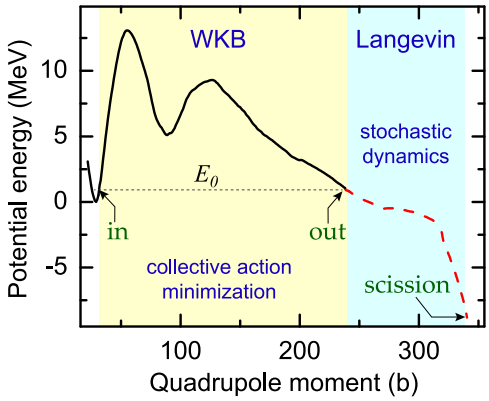

FIG. 1. Potential energy of ^{240}Pu calculated along the most probable path to fission. In the classically forbidden region (marked WKB; between the inner turning point "in" and outer turning point "out"), the collective action (1) is minimized to determine the half-life. Outside the outer turning point and scission, the evolution of the system is given by stochastic Langevin dynamics.

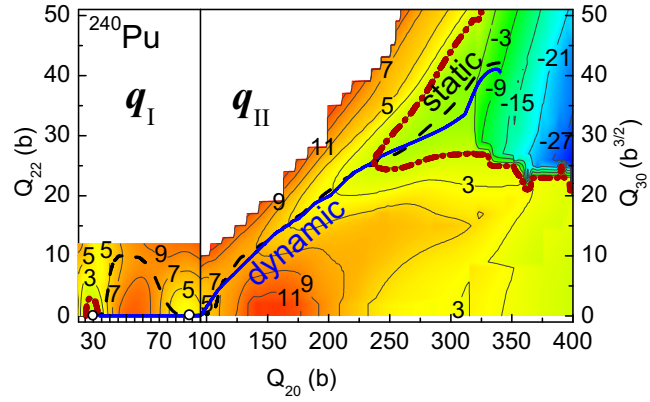

FIG. 2. Projections of the static (dashed line) and dynamic (solid line) SF paths on the potential energy contours in the two considered regions $\boldsymbol{q}_{\rm I}$ and $\boldsymbol{q}_{\rm II}$ of the collective space. The contours of inner and outer turning points are shown by dash-dotted lines. Ground-state and fission-isomer minima are marked by dots.

that pairing dynamics can profoundly impact penetration probabilities by restoring symmetries spontaneously broken in the static approach.

In this study, we predict for the first time mass and charge distributions in SF within a unified theoretical framework schematically illustrated in Fig. 1. We employ state-of-the-art DFT to compute adiabatic PESs and collective inertia in a multidimensional space of collective coordinates. This allows us to predict the tunneling probabilities along the hypersurface of outer turning points and solve the Langevin equations to propagate the nucleus from the outer turning points to scission. The validity of such an approach is illustrated in the benchmark case of ^{240}Pu, where the experimental fission yields are well known [37–39].

Theoretical framework. We calculate the SF half-life by following the formalism described in Ref. [34]. In the WKB approximation, the half-life can be written as $T_{1/2} = \ln 2/(nP)$ [40,41], where n is the number of assaults on the fission barrier per unit time (we adopt the standard value of $n = 10^{20.38}$ s^{-1}) and $P = 1/(1+e^{2S})$ is the penetration probability expressed in terms of the action integral,

$$S(L) = \int_{s_{\rm in}}^{s_{\rm out}} \sqrt{\frac{2\mathcal{M}_{\rm eff}(s)}{\hbar^2}(V(s)-E_0)}\,ds, \qquad (1)$$

calculated along the optimum fission path $L(s)$ connecting the inner and outer turning points $s_{\rm in}$ and $s_{\rm out}$ within a multidimensional collective space characterized by N collective variables $\boldsymbol{q} = (q_1,\ldots,q_N)$. The effective inertia $\mathcal{M}_{\rm eff}(s)$ is obtained from the nonperturbative cranking inertia tensor $\mathcal{M}_{ij}$ [34,40–42]. The potential along the path is $V(s)$, and E_0 stands for the collective ground-state energy; see Fig. 1.

At first, we compute the PES $V(\boldsymbol{q})$ of the nucleus by solving the Hartree-Fock-Bogoliubov equations with constraints on $\boldsymbol{q}$. In order to stay consistent with our previous studies, we use the SkM* parametrization [43] of the Skyrme energy density and a density-dependent mixed-type pairing term [44]. The pairing strength is locally adjusted to reproduce odd-even mass differences [45]. Without missing crucial physics, we divide the collective space into two three-dimensional (3D) regions to improve the numerical efficiency of the calculation. In the region of elongations between the ground state and fission isomer, the most relevant degrees of freedom are the elongation, represented by the mass quadrupole moment Q_{20}; triaxiality, represented by the mass quadrupole moment Q_{22}; and the coordinate λ_2 representing dynamic pairing fluctuations [36]. This results in a 3D space $\boldsymbol{q}_{\rm I} \equiv (Q_{20}, Q_{22}, \lambda_2)$. For elongations greater than that of the fission isomer, triaxiality plays a minor role, but reflection-asymmetric degrees of freedom, represented by the mass octupole moment Q_{30}, become important; hence, in that region, our collective space is $\boldsymbol{q}_{\rm II} \equiv (Q_{20}, Q_{30}, \lambda_2)$. In practical calculations, it is convenient to introduce dimensionless coordinates $\{x_i\}$, where $x_i = q_i/\delta q_i$ and δq_i are the scale parameters that are also used when determining numerical derivatives of density matrices. Here, we employ the values of δq_i as in Refs. [36,46].

The potential energy and inertia tensor are computed with the symmetry-unrestricted DFT solver HFODD (v2.49t) [47]. The potential is corrected by subtracting the zero-point energy computed within the Gaussian overlap approximation [11,48,49]. The derivatives of the density matrix with respect to the collective coordinates, which are needed to compute the nonperturbative cranking inertia tensor, are calculated with the finite difference method [46]. In Fig. 2, we show the projections of the most probable fission path in the two-dimensional planes $\{Q_{20}, Q_{22}\}$ and $\{Q_{20}, Q_{30}\}$. For all pairs of inner and outer turning points at energy E_0, the one-dimensional path $L(s)$ is calculated with the dynamic programming method [40] by minimizing the action in the multidimensional space of $\{x_i\}$. In this way, we obtain a family of SF probabilities $P(s_{\rm out})$ that correspond to the hypersurface of outer turning points $s_{\rm out}$.

For all the points $s_{\rm out}$, we then compute the time-dependent fission path to scission by solving the dissipative Langevin

equations [33,50]:

$$\frac{dp_i}{dt} = -\frac{p_j p_k}{2}\frac{\partial}{\partial x_i}(\mathcal{M}^{-1})_{jk} - \frac{\partial V}{\partial x_i} - \eta_{ij}(\mathcal{M}^{-1})_{jk}p_k + g_{ij}\Gamma_j(t),$$
$$\frac{dx_i}{dt} = (\mathcal{M}^{-1})_{ij}p_j, \quad (2)$$

where p_i represents the momentum conjugate to x_i, η_{ij} is the dissipation tensor, $g_{ij}\Gamma_j(t)$ is the random (Langevin) force with $\Gamma_j(t)$ being a time-dependent stochastic variable with a Gaussian distribution, and g_{ij} is the random-force strength tensor. The time-correlation property of the random force is assumed to follow the relation $\langle\Gamma_k(t)\Gamma_l(t')\rangle = 2\delta_{kl}\delta(t-t')$. The strength of the random force is related to the dissipation coefficients through the fluctuation-dissipation theorem: $\sum_k g_{ik}g_{jk} = \eta_{ij}k_{\rm B}T$, where the temperature T of the fissioning nucleus at any instant of its evolution is given by $k_{\rm B}T = \sqrt{E^*/a}$. Here, $a = A/10$ MeV^{-1} is the level density parameter and $E^* = V(s_{\rm out}) - V(\boldsymbol{x}) - \frac{1}{2}\sum(\mathcal{M}^{-1})_{ij}p_i p_j$ represents the excitation energy of the fissioning system system in the classically allowed region; for SF, E^* increases as the system moves toward scission beyond $s_{\rm out}$. Scission is defined here by the criterion that the number of particles (N_q) in the neck between the two prefragments be less than 0.5. Each point on the scission hypersurface defines a split corresponding to two fission fragments. The mass and charge of the fragments are obtained from the calculated density distributions [45]. Owing to the random force in the Langevin equations, repeating the calculation several times with the same initial condition at a given outer turning point $s_{\rm out}$ yields different trajectories: The charge and mass distribution are then simply obtained by counting the number of trajectories ending at a given fragmentation, weighing with $P(s_{\rm out})$, and normalizing the result to unit probability. Finally, to account for fluctuations of particle number in the neck at scission, Langevin yields are convoluted with a Gaussian of width σ [51]. Based on the expectation value of the total (proton) particle number in the neck region, we choose $\sigma = 3$ (or 2) for A (or Z).

Compared to the Brownian shape-motion approach, which is applied to describe induced fission [17–19], our model contains a number of attractive theoretical features: (i) It is based on a self-consistent theory utilizing realistic effective interactions both in particle-hole and particle-particle channels; (ii) the fission pathway is obtained by an explicit minimization of the collective action, i.e., the static assumption is not used; (iii) the inertial effects are considered both during tunneling and Langevin propagation; and (iv) the full Langevin description of the nuclear shape dynamics is considered.

Results. The initial collective energy E_0 is a crucial quantity for determining the fission half-life. To find E_0, we first calculate the most probable fission path of ^{240}Pu by minimizing the action (1) in the 3D + 3D space described above. An agreement with the experimental SF half-life [37] is achieved for $E_0 = 0.97$ MeV, which is indeed very close to a value of 1 MeV assumed in our previous work [34,36]. In the following, we adopt the value $E_0 = 0.97$ MeV to define the inner and outer turning points. As shown in Fig. 2 and discussed in detail in our previous work [36], the least-action path between the ground-state and fission isomer in ^{240}Pu is axially symmetric, and it dramatically differs from the static trajectory corresponding to the least-energy path, which goes through triaxial shapes. In the region $\boldsymbol{q}_{\rm II}$, the dynamic path is predicted to be very close to the static path. Note that in Fig. 2, the part of the dynamic path outside the outer turning point is calculated by disregarding the random force in Eq. (2); this enforces deterministic trajectories (see also below).

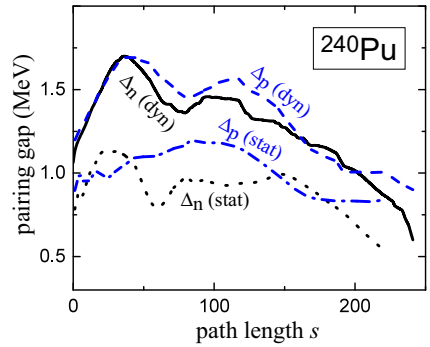

FIG. 3. Variation of the pairing gap for neutrons and protons along the static and dynamic paths of Fig. 2.

In general, we found that the impact of nuclear pairing on $S(L)$ becomes strongly reduced at large deformations and the pairing gaps attain the static values near the outer turning point. This is because the most probable fission pathways can be associated with shapes characterized by large symmetry breaking. This observation is demonstrated in Fig. 3 for the dynamic and static paths of Fig. 2 by showing the neutron and proton pairing gaps along the path length s. Subsequently, we

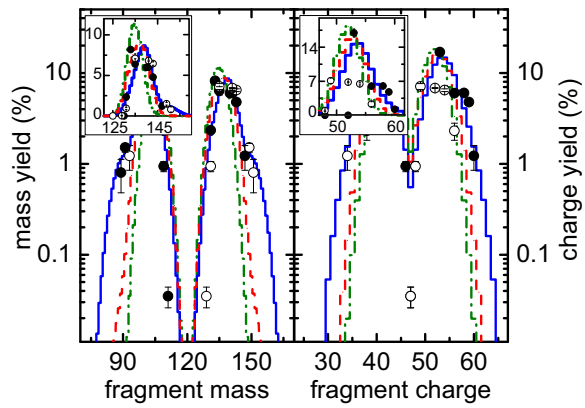

FIG. 4. Mass (left) and charge (right) yield distributions for the SF of ^{240}Pu. The experimental values [38,39] (mirror points) are shown by solid (open) circles. Calculations with dissipative Langevin dynamics and full inertia (solid blue lines) are compared to results obtained with nondissipative dynamics and full inertia (red dashed lines) and with dissipative dynamics and a diagonal unit inertia tensor (green dashed-dotted lines). The insets shows the yields in a linear scale.

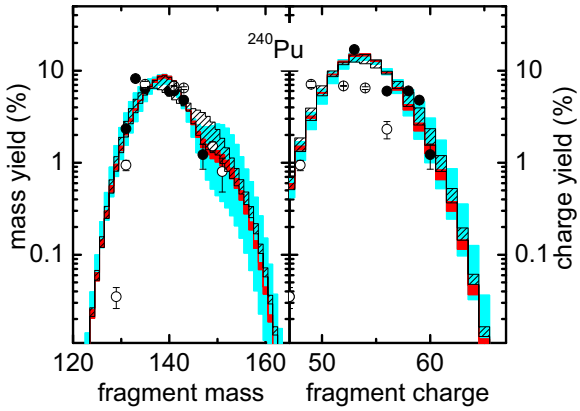

FIG. 5. Mass (left) and charge (right) distributions of heavier SF yields of ^{240}Pu. The symbols are the same as in Fig. 4. The shaded regions are uncertainties in the distributions due to variations in E_0 (narrow red band), dissipation tensor (wider cyan band), and scission configuration (linear hatch pattern).

restrict the dynamical space in the classically allowed region to the surface defined by $\{Q_{20}, Q_{30}\}$. In the following, we calculate the fission paths on this surface for a collection of 900 outer turning points around the most probable s_{out}.

The Langevin propagation is studied in three different scenarios. In the first variant, the mass and charge distributions of fission fragments are computed without invoking dissipation and fluctuation by setting $\eta_{ij} = 0$ (thus $g_{ij} = 0$). Under such conditions, the Langevin equations resemble the deterministic Newtonian equations of motion with a one-to-one correspondence between outer turning points and scission points. By computing 900 trajectories to scission, we obtain mass and charge yield distributions marked by the red dashed line in Fig. 4. The most probable values of the fission yields are consistent with the data but the distribution tails are clearly off. In the second variant, we incorporate a constant collective dissipation tensor η_{ij} with reasonable values $\eta_{11} = 50\hbar$, $\eta_{22} = 40\hbar$, and $\eta_{12} = 5\hbar$, but take a diagonal unit mass tensor and obtain the green dashed-dotted line. In this case, fission dynamics is dominated by the static features of the PES. However, since the excitation energy is small, dissipation effects are weak. As a result, the distribution width is even narrower than in the first variant. It is only by combining a constant dissipation tensor with the nonperturbative cranking inertia that we obtain the solid blue lines, which nicely agree with experiment over the whole range of mass-charge splits. The results shown in Fig. 4 correspond to 100 different runs per each outer turning point, hence the distributions contain contribution from 90 000 trajectories.

To illustrate the sensitivity of yield distributions to the initial collective energy E_0, the narrow red band in Fig. 5 shows the distribution uncertainty when taking a sample of 11 different values of E_0 within the range $0.7 \leqslant E_0 \leqslant 1.2$ MeV. While such a variation in E_0 changes the SF half-life by over two orders of magnitude, its impact on fission yield distributions is minimal. The wider cyan band shows the spread in predicted distributions when sampling the dissipation tensor in the range of $0 \leqslant \eta_{12} \leqslant 30\hbar$ and $(\eta_{11}, \eta_{22}) \in [30\hbar, 400\hbar]$ with the constraint $1 \leqslant \eta_{11}/\eta_{22} \leqslant 1.25$. Note that we consider a very broad range of variations in order to account for the uncertainties in the theoretical determination the dissipation tensor. Finally, the linear pattern in Fig. 5 indicates the uncertainty related to the definition of scission configurations and corresponds to $0.3 \leqslant N_q \leqslant 2.0$. It is very encouraging to see that the predicted yield distributions vary relatively little, even for nonphysically large values of η_{ij} and N_q. We have also found that the distributions are practically indistinguishable when the level density parameter a varies from $A/8$ to $A/13$.

Conclusions. In this work, we propose a microscopic approach rooted in nuclear DFT to calculate mass and charge distributions of SF yields. The SF penetrabilities, obtained by minimizing the collective action in large multidimensional PESs with realistic collective inertia, are used as inputs to solve the time-dependent dissipative Langevin equations. By combining many trajectories connecting the hypersurface of outer turning points with the scission hypersurface, we predict SF yield distributions. The results of our pilot calculations for ^{240}Pu are in excellent agreement with experiment and remain reasonably stable under large variations of input parameters. This is an important outcome, as SF yield distributions are important observables for benchmarking theoretical models of SF [52]. This finding is reminiscent of the analysis of Ref. [17] for low-energy neutron- and γ-induced fission, which found that the yield distributions predicted in the Brownian-motion approach are insensitive to large variations of dissipation tensor. On the other hand, according to our analysis, the collective inertia tensor impacts both tunneling and the Langevin dynamics.

The results of our study confirm that the PESs is the most important ingredient when it comes to the maxima of yield distributions. This is consistent with the previous DFT studies of most probable SF splits [31,53–56], which indicate that the topology of the PES in the prescission region is the crucial factor. On the other hand, both dissipative collective dynamics and collective inertia are essential when it comes to the shape of the yield distributions. The fact that the predictions are fairly robust with respect to the details of dissipative aspects of the model is most encouraging.

Acknowledgments. Discussions with A. Baran, J. Dobaczewski, J. A. Sheikh, and S. Pal are gratefully acknowledged. This work was supported by the U.S. Department of Energy, Office of Science, Office of Nuclear Physics under Awards No. DOE-DE-NA0002574 (the Stewardship Science Academic Alliances program) and No. DE-SC0008511 (NUCLEI SciDAC-3 collaboration). Part of this research was performed under the auspices of the U.S. Department of Energy by Lawrence Livermore National Laboratory under Contract No. DE-AC52-07NA27344. Computational resources were provided through an INCITE award, "Computational Nuclear Structure," by the National Center for Computational Sciences (NCCS) and by the National Institute for Computational Sciences (NICS). Computing resources were also provided through an award by the Livermore Computing Resource Center at Lawrence Livermore National Laboratory.

[1] G. Flerov and K. Petrzhak, Phys. Rev. **58**, 89 (1940).
[2] S. Nilsson, C. Tsang, A. Sobiczewski, Z. Szymański, S. Wycech, C. Gustafson, I.-L. Lamm, P. Möller, and B. Nilsson, Nucl. Phys. A **131**, 1 (1969).
[3] G. Seaborg and W. Loveland, *The Elements beyond Uranium* (Wiley-Interscience, New York, 1990).
[4] Y. T. Oganessian, J. Phys. G **34**, R165 (2007).
[5] I. Panov, E. Kolbe, B. Pfeiffer, T. Rauscher, K. Kratz, and F. Thielemann, Nucl. Phys. A **747**, 633 (2005).
[6] J. Beun, G. C. McLaughlin, R. Surman, and W. R. Hix, Phys. Rev. C **77**, 035804 (2008).
[7] J. Erler, K. Langanke, H. P. Loens, G. Martinez-Pinedo, and P.-G. Reinhard, Phys. Rev. C **85**, 025802 (2012).
[8] S. Goriely, J.-L. Sida, J.-F. Lemaître, S. Panebianco, N. Dubray, S. Hilaire, A. Bauswein, and H.-T. Janka, Phys. Rev. Lett. **111**, 242502 (2013).
[9] A. Nichols, D. Aldama, and M. Verpelli, *Handbook for nuclear data for safeguards: Database extensions, August 2008*, Tech. Rep. INDC(NDS)-0534, International Atomic Energy Agency, Vienna, 2008 (unpublished).
[10] R. Murray and K. Holbert, *Nuclear Energy: An Introduction to the Concepts, Systems, and Applications of Nuclear Processes* (Elsevier, Oxford, UK, 2014).
[11] A. Staszczak, A. Baran, and W. Nazarewicz, Phys. Rev. C **87**, 024320 (2013).
[12] S. A. Giuliani, L. M. Robledo, and R. Rodríguez-Guzmán, Phys. Rev. C **90**, 054311 (2014).
[13] S. A. Giuliani and L. M. Robledo, Phys. Rev. C **88**, 054325 (2013).
[14] C. Xu and Z. Ren, Phys. Rev. C **71**, 014309 (2005).
[15] A. Bonasera and A. Iwamoto, Phys. Rev. Lett. **78**, 187 (1997).
[16] T. Ichikawa, A. Iwamoto, and P. Möller, Phys. Rev. C **79**, 014305 (2009).
[17] J. Randrup, P. Möller, and A. J. Sierk, Phys. Rev. C **84**, 034613 (2011).
[18] J. Randrup and P. Möller, Phys. Rev. C **88**, 064606 (2013).
[19] P. Möller and J. Randrup, Phys. Rev. C **91**, 044316 (2015).
[20] A. V. Andreev, G. G. Adamian, N. V. Antonenko, and A. N. Andreyev, Phys. Rev. C **88**, 047604 (2013).
[21] J.-F. Lemaître, S. Panebianco, J.-L. Sida, S. Hilaire, and S. Heinrich, Phys. Rev. C **92**, 034617 (2015).
[22] S. Panebianco, J.-L. Sida, H. Goutte, J.-F. Lemaître, N. Dubray, and S. Hilaire, Phys. Rev. C **86**, 064601 (2012).
[23] B. D. Wilkins, E. P. Steinberg, and R. R. Chasman, Phys. Rev. C **14**, 1832 (1976).
[24] W. Swiatecki and S. Bjørnholm, Phys. Rep. **4**, 325 (1972).
[25] A. K. Kerman and S. E. Koonin, Phys. Scr. **10**, 118 (1974).
[26] S. Levit, Phys. Rev. C **21**, 1594 (1980).
[27] J. W. Negele, Rev. Mod. Phys. **54**, 913 (1982).
[28] J. Skalski, Phys. Rev. C **76**, 044603 (2007).
[29] S. Levit, J. W. Negele, and Z. Paltiel, Phys. Rev. C **22**, 1979 (1980).
[30] C. Simenel and A. S. Umar, Phys. Rev. C **89**, 031601(R) (2014).
[31] G. Scamps, C. Simenel, and D. Lacroix, Phys. Rev. C **92**, 011602 (2015).
[32] Y. Tanimura, D. Lacroix, and G. Scamps, Phys. Rev. C **92**, 034601 (2015).
[33] Y. Abe, S. Ayik, P. G. Reinhard, and E. Suraud, Phys. Rep. **275**, 49 (1996).
[34] J. Sadhukhan, K. Mazurek, A. Baran, J. Dobaczewski, W. Nazarewicz, and J. A. Sheikh, Phys. Rev. C **88**, 064314 (2013).
[35] J. Zhao, B.-N. Lu, T. Nikšić, and D. Vretenar, Phys. Rev. C **92**, 064315 (2015).
[36] J. Sadhukhan, J. Dobaczewski, W. Nazarewicz, J. A. Sheikh, and A. Baran, Phys. Rev. C **90**, 061304 (2014).
[37] P. Salvador-Castiñeira, T. Bryś, R. Eykens, F.-J. Hambsch, A. Moens, S. Oberstedt, G. Sibbens, D. Vanleeuw, M. Vidali, and C. Pretel, Phys. Rev. C **88**, 064611 (2013).
[38] J. Laidler and F. Brown, J. Inorg. Nucl. Chem. **24**, 1485 (1962).
[39] H. Thierens, A. De Clercq, E. Jacobs, D. De Frenne, P. D'hondt, P. De Gelder, and A. J. Deruytter, Phys. Rev. C **23**, 2104 (1981).
[40] A. Baran, K. Pomorski, A. Lukasiak, and A. Sobiczewski, Nucl. Phys. A **361**, 83 (1981).
[41] A. Baran, Phys. Lett. B **76**, 8 (1978).
[42] A. Baran, Z. Łojewski, K. Sieja, and M. Kowal, Phys. Rev. C **72**, 044310 (2005).
[43] J. Bartel, P. Quentin, M. Brack, C. Guet, and H.-B. Håkansson, Nucl. Phys. A **386**, 79 (1982).
[44] J. Dobaczewski, W. Nazarewicz, and M. Stoitsov, Eur. Phys. J. A **15**, 21 (2002).
[45] N. Schunck, D. Duke, H. Carr, and A. Knoll, Phys. Rev. C **90**, 054305 (2014).
[46] A. Baran, J. A. Sheikh, J. Dobaczewski, W. Nazarewicz, and A. Staszczak, Phys. Rev. C **84**, 054321 (2011).
[47] N. Schunck, J. Dobaczewski, J. McDonnell, W. Satuła, J. Sheikh, A. Staszczak, M. Stoitsov, and P. Toivanen, Comput. Phys. Commun. **183**, 166 (2012).
[48] A. Staszczak, S. Piłat, and K. Pomorski, Nucl. Phys. A **504**, 589 (1989).
[49] A. Baran, A. Staszczak, J. Dobaczewski, and W. Nazarewicz, Int. J. Mod. Phys. E **16**, 443 (2007).
[50] P. Fröbrich and I. Gontchar, Phys. Rep. **292**, 131 (1998).
[51] W. Younes and D. Gogny, Tech. Rep. LLNL-TR-586678, Lawrence Livermore National Laboratory (LLNL), Livermore, CA, 2012 (unpublished).
[52] G. F. Bertsch, W. Loveland, W. Nazarewicz, and P. Talou, J. Phys. G **42**, 077001 (2015).
[53] A. Staszczak, A. Baran, J. Dobaczewski, and W. Nazarewicz, Phys. Rev. C **80**, 014309 (2009).
[54] M. Warda, A. Staszczak, and W. Nazarewicz, Phys. Rev. C **86**, 024601 (2012).
[55] J. D. McDonnell, W. Nazarewicz, and J. A. Sheikh, Phys. Rev. C **87**, 054327 (2013).
[56] J. D. McDonnell, W. Nazarewicz, J. A. Sheikh, A. Staszczak, and M. Warda, Phys. Rev. C **90**, 021302 (2014).